Available online at www.sciencedirect.com

ScienceDirect

Procedia IUTAM 14 (2015) 201 – 210

Procedia IUTAM

www.elsevier.com/locate/procedia

IUTAM_ABCM Symposium on Laminar Turbulent Transition

Modeling three dimensional effects on cross flow instability from leading edge dimples

Richard Ashworth*, Shahid Mughal†

*Airbus Group Innovations, Bristol BS34 7QW, UK
†Imperial College, London SW7 2AZ, UK

Abstract

The formation of shallow dimples near the leading edge of natural laminar flow wings can occur during operation due to impact by hail, potentially changing the stability characteristics and causing an early transition to turbulence downstream of the dimple. Changes in the base flow will be strongly three-dimensional in character putting this problem beyond the capability of the standard strip based approaches founded on conical flow assumptions that are routinely used in the aerospace industry. This paper describes the application of a fully 3d method to a dimple on a wing for flow resembling that on a natural laminar flow wing. Solving the three-dimensional compressible boundary layer equations for the base flow and using a point to point marching scheme for solving the 3d PSE equations, it is shown that high wave-number stationary cross-flow modes can become unstable and grow rapidly in the dimple wake in a region well beyond the leading edge where stationary cross-flow modes would normally be decaying.

Keywords: Parabolized Stability Equations; Cross-flow instability, Boundary layer equations, Natural laminar flow, Marching in planes PSE3D, Dimple, Biglobal instability, Biglobal PSE, PSE3D

* Corresponding author. Tel.: +44 163714497.
*E-mail address:*richard.ashworth@airbus.com

doi:10.1016/j.piutam.2015.03.041

1. Introduction

The design of swept natural laminar flow wings is driven by the need to simultaneously control the growth of stationary cross-flow instabilities arising particularly near the leading edge and the growth of Tollmein Schlichting instabilities over the wing-box. The control of cross-flow instabilities is achieved in part by reducing the cross-flow though reduced sweep compared to conventional turbulent wings. This comes at the cost of increased wave drag and thus requires a reduced design cruise velocity compared to higher sweep turbulent wings in order to maintain acceptable levels of wave drag. Optimal performance thus requires that design margins for controlling instabilities are reduced to a minimum and it is vitally important that environmental factors that can degrade performance are accurately modelled and well understood. Amongst these factors is leading edge damage caused by hard impacts such as through hail. The effect of such impacts will generally be to introduce a concave dimple like region in the wing surface introducing strongly three-dimensional effects into the boundary layer in the vicinity and wake of the dimple.

Standard industrial design tools for turbulent transition modelling in aerospace take advantage of the near conical flow conditions that pertain across much of the span of typical clean wings. Thus a 2d strip approach can be adopted in which, typically, a RANS solution provides pressure conditions to drive a 2d (or swept tapered) boundary layer solver for the base flow. Local stability analysis is usually applied to the base flow in conjunction with a critical N factor to determine transition. The state of the art, in terms of instability analysis of boundary-layers, would be represented by the use of the Parabolised Stability Equations (PSE) model of Herbert[1,2], by invoking the infinite swept type approximation, to treat span-wise variations of the basic flow as being of locally infinite sweep like and thus assuming the span-wise wave-number β remains fixed during the PSE computations.

Clearly the standard industrial approach is not adequate for assessing the effect of leading edge dimples. The work described in this paper demonstrates the application of a fully three dimensional approach based on the developments of Mughal[3] and Arthur, Horton & Mughal[4] where the PSE formulation was extended to deal with truly varying 3D flows. These include the use of a three-dimensional boundary layer solver for computation of the base flow and a fully three-dimensional non-local approach based on solution of the parabolised stability equations in generalised non-orthogonal co-ordinates for the stability analysis. The latter equation set is solved through an efficient point to point marching scheme making its solution for multiple modes in order to generate N factor envelopes a practical possibility in engineering applications.

This paper describes the application of these fully 3d methods to an infinite swept wing test case under conditions resembling those on a natural laminar flow wing. Numerical computations of the mean flow about the wing and its stability properties with respect to stationary cross-flow vortices have been performed for dimples of various sizes imposed near the leading edge of the wing. The paper describes this analysis for one particular dimple size which results in high wave-number cross-flow instability modes in the wake of the dimple from about 20% chord. This is a region of the flow that would otherwise be highly stable with respect to stationary cross-flow vortices. It is seen that these instabilities are not captured by the strip methods routinely used in industry.

2. Numerical Approach

2.1. Boundary Layer Solver

The compressible boundary layer (BL) equations have been solved in a body fitted orthogonal co-ordinate system as shown in equations (1-3), where variables (U,V,W) are the velocity components, ρ the density, μ the viscosity and suffix e denotes the boundary-layer edge. For brevity the energy equation is not shown, as this is the standard form (see Cebeci & Cousteix[5]). The pressure field P_e is computed by a fully 3D-Reynolds Averaged Navier Stokes (RANS) method, and of note is that variations in the surface pressures in both span and stream-wise directions arise. The BL equation set which is hyperbolic in the surface tangential directions and elliptic in the wall normal direction is solved through a marching procedure across the wing surface, requiring inflow conditions along the attachment line and the inboard edge of the domain. These are obtained by solving the attachment line problem along the leading edge and use of an infinite swept approximation (zero span gradients) along the inboard and outboard edge. In the interior of the domain second order accurate 3 point schemes are used for the normal to leading edge and wall

normal directions whilst for the span direction the discretisation is accomplished through a combination of schemes to correctly account for the zone of dependence for span reversing flow. Output from the boundary layer solver includes all the base flow profile data required for the PSE analysis.

$$\frac{\partial(\rho U)}{\partial \xi}+\frac{\partial(\rho V)}{\partial \eta}+\frac{\partial(\rho W)}{\partial \zeta}=0, \tag{1}$$

$$\rho\left(U\frac{\partial U}{\partial \xi}+U\frac{\partial U}{\partial \eta}+U\frac{\partial U}{\partial \zeta}\right)=-\frac{\partial P_e}{\partial \xi}+\frac{\partial}{\partial \eta}\left(\mu\frac{\partial U}{\partial \eta}\right), \tag{2}$$

$$\rho\left(U\frac{\partial W}{\partial \xi}+U\frac{\partial W}{\partial \eta}+U\frac{\partial W}{\partial \zeta}\right)=-\frac{\partial P_e}{\partial \zeta}+\frac{\partial}{\partial \eta}\left(\mu\frac{\partial W}{\partial \eta}\right). \tag{3}$$

2.2. 3d PSE point to point marching scheme (PPM-PSE3D)

Solution of the PSE's for boundary layer disturbances is a practical engineering alternative to local stability theory (LST) based eigenvalue analysis of the Orr-Sommerfeld equations. It overcomes the restrictions of the parallel flow assumption inherent in the latter whilst retaining the benefit of very low computational cost compared to direct numerical simulation, as well as capturing non-parallel and surface curvature effects, also ignored in LST analysis. The method is based on a decomposition of the disturbance into a slowly varying amplitude function and local wave factor

$$q'(\xi,\eta,\zeta,t)=q(\xi,\eta,\zeta)\exp\left[\mathrm{i}(\theta(\xi,\zeta)-\omega t)\right], \tag{4}$$

resulting in complex wave-number components and an irrotationality condition to be satisfied,

$$\alpha=\alpha_r+i\alpha_i=\frac{\partial\theta}{\partial\xi},\qquad \beta=\beta_r+i\beta_i=\frac{\partial\theta}{\partial\zeta},\qquad \frac{\partial\alpha}{\partial\zeta}=\frac{\partial\beta}{\partial\xi}. \tag{5}$$

The resultant parabolised stability equation for the amplitude function can be written in the generic form,

$$Lq+M\frac{1}{h_1}\frac{\partial q}{\partial \xi}+N\frac{1}{h_2}\frac{\partial q}{\partial \zeta}=0, \tag{6}$$

in which L, M and N are differential matrix operators in the wall normal direction and h_1 and h_2 are metric factors arising from the use of a general non-orthogonal body-fitted co-ordinate system (ξ,η,ζ). The system of equations is closed through the use of integral norm over the body surface, *i.e.*

$$\int_0^\infty q^*\left(\partial q/\partial\xi\right)\,d\eta\Big/\int_0^\infty\left(q^*q\right)\,d\eta=0, \tag{7}$$

where * indicates the adjoint. This allows the stream-wise wave-number α to be determined, while the irrotationality condition is used to capture span-wise changes to the wave-number β. Full details of the implementation are described by Mughal[3], essentially equations (6) are solved using a point to point upwind marching scheme in the

interior of the computation domain. On the inboard and outboard boundaries ($\zeta=\zeta_{min}$ and $\zeta=\zeta_{max}$) an infinite swept assumption is utilised to march the solution in a 2d manner from the upstream point ($\xi=\xi_{min}$). For each point an iterative procedure is followed to convergence in which the normalisation condition (7) is used to update α according to,

$$\alpha_k = \alpha_{k-1} + \int_0^\infty q^* \left(\partial q/\partial \xi\right) d\eta \Bigg/ \int_0^\infty \left(q^* q\right)\ d\eta, \tag{8}$$

followed by a correction of β from the irrotationality condition. Currently the method defines N factors in terms of disturbance amplitude ratios for pairs of points (s_0, s) along lines of constant ζ. Thus integrating growth rates gives,

$$N = \frac{q'}{q'_0} = \mathrm{R}\int_{s_0}^{s} \left(i\frac{\partial \theta}{\partial \xi} + \frac{1}{q}\frac{\partial q}{\partial \xi} \right) d\xi \cong \int_{s_0}^{s} (-\alpha_i)\, d\xi, \tag{9}$$

in which the final approximation on the right hand side is based on the neglect of the amplitude derivative term, which is generally assumed to be small, since most of the rapid change is absorbed and captured in the determination of α.

2.3. 3d PSE marching in planes scheme (MiP-PSE3D)

The previously described method enables solution of the fully 3d parabolised stability equations in an efficient manner for the development of span-wise periodic modes under conditions in which the base flow is three-dimensional. How strong a three-dimensional varying flow the approach can deal with is an open issue which we plan on investigating in future. The development of more general bi-global modes, for strongly varying 3d basic flows, can be tackled with the marching in planes method. In this approach the Orr-Sommerfeld operator, L, in equation (6) and the span-wise derivative terms are replaced with a bi-global elliptic operator L_2, via the ansatz *;*

$$q'\left(\xi,\eta,\zeta,t\right) = q\left(\xi,\eta,\zeta\right)\exp\left[\mathrm{i}\left(\alpha\xi - \omega t\right)\right], \tag{10}$$

where α now represents a globally averaged wave-number and growth measure of the disturbance, thus the parabolised stability equations become,

$$L_2 q + M\frac{1}{h_1}\frac{\partial q}{\partial \xi} = 0. \tag{11}$$

The integral norm condition in (7) is replaced with a single double integral condition over a plane.

$$\frac{\iint q^* \left(\partial q/\partial \xi\right) d\eta d\zeta}{\iint \left(q^* q\right) d\eta d\zeta} = 0. \tag{12}$$

As before an iterative scheme is employed in which an update to the global wave-number and growth rate for the state is evaluated from

$$\alpha_k = \alpha_{k-1} + \frac{\iint q^*\left(\partial q/\partial \xi\right) d\eta d\zeta}{\iint \left(q^* q\right) d\eta d\zeta}. \tag{13}$$

This method is generally an order of magnitude more computationally intensive than the PPM-PSE3D scheme and would not normally be used to calculate the development of span periodic modes except in order to provide confidence through agreement in the solutions obtained by the two methods and or where the basic flow has strong variations in the third span-wise directions. Presently, we use both approaches for validation purposes and as a means to investigate merits of the two radically different techniques. For this purpose, to compare results, local wave-number and growth rates can then be defined from the global rate by the relation

$$\alpha_{\text{local}} = \alpha_{\text{global}} + \left. \frac{\int_0^\infty q^*\left(\partial q/\partial \xi\right) d\eta}{\int_0^\infty \left(q^* q\right) d\eta} \right|_{\zeta_{local}}, \tag{14}$$

on choosing a convenient ξ direction. We presently choose this to be in the normal to wing-leading-edge direction, in order to make quantitative comparison with the point-point marching PSE3D scheme; though this is an open question as to which direction to take when extracting local growth rates from some globally averaged definition of α as defined by equation (13).

3. Computations

3.1. Test case and computational model

The M2355 variable sweep symmetric aerofoil model[6] with normal to leading edge chord 0.43m has been extensively tested in the ARA transonic wind-tunnel, (see Fig 1) and is designed to produce span invariant flow in the mid span region. For a sweep of 25 degrees and zero incidence at M=0.7 (Re=5.0x10^6) conditions resembling those on a natural laminar flow wing are generated on the upper surface.

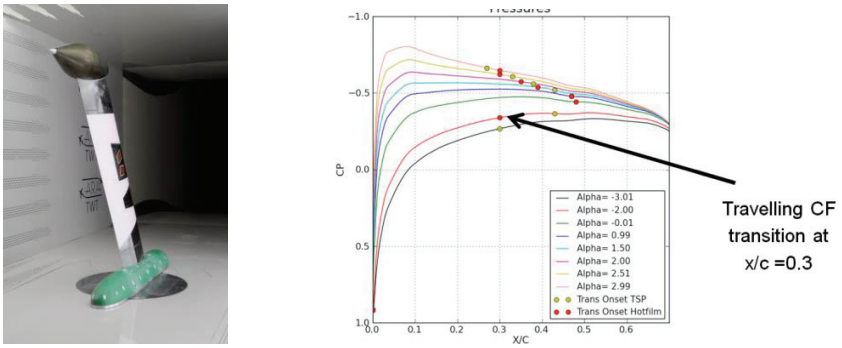

Fig. 1. M2355 model in ARA tunnel (left) and upper surface Cp distribution and transition at range of incidences (right).

3.2. Computational model for wing and dimple

The tunnel model has been represented in RANS computations as an infinite swept configuration in an open flow. The 3d SOLAR[7] mesh for the computations was obtained from a hybrid 2d mesh through extrusion across the span with variable spacing to give the required resolution in the intended dimple region (Fig, 2). The dimple itself was introduced into the clean mesh through mesh deformation. RANS solutions were obtained on the mesh with the DLR Tau flow solver fixing transition at 50% chord and using a second order central scheme for convective fluxes. A number of similar meshes with different dimple sizes have been used. Results for one particular set of dimple parameters as shown in Fig. 2 are focused on for the remainder of this paper.

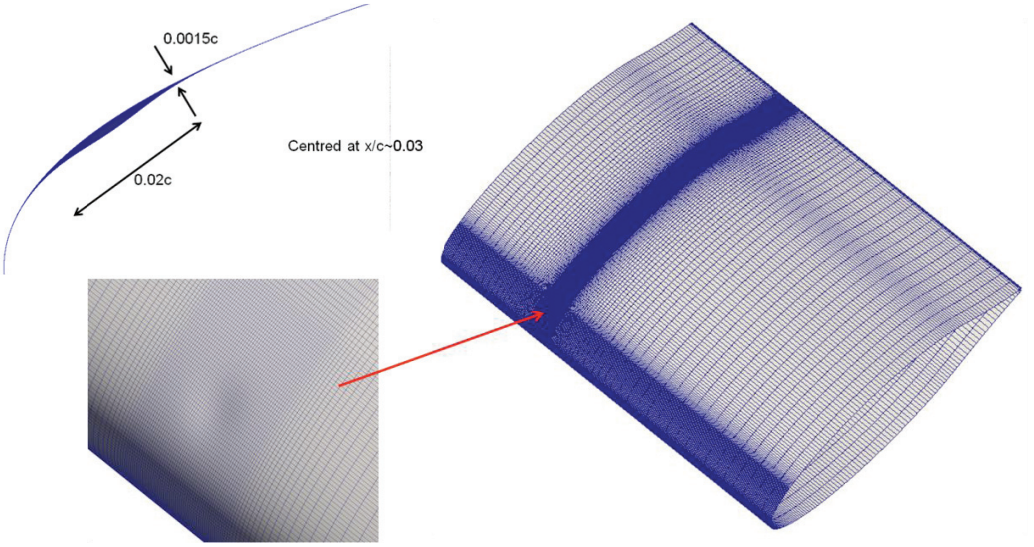

Fig. 2. Details of RANS surface mesh and dimple.

The dimple has been centered at a location approximately in chord units x/c=0.03 from the leading edge, downstream of the neutral stability location for all stationary cross-flow modes. The dimple diameter in chord units, D/c=0.02, is significantly larger than the wavelength of any unstable modes and the depth in chord units at d/c=0.0015 is near the maximum for which the flow remains attached everywhere.

Surface pressure coefficient values on slices orthogonal to the leading edge were extracted through surface reconstruction and interpolation to points in the slices from the RANS mesh (see Fig 3). A bespoke preprocessor for the boundary layer solver was used to generate edge conditions and attachment line for a 3d boundary layer mesh ready for running the boundary layer solver.

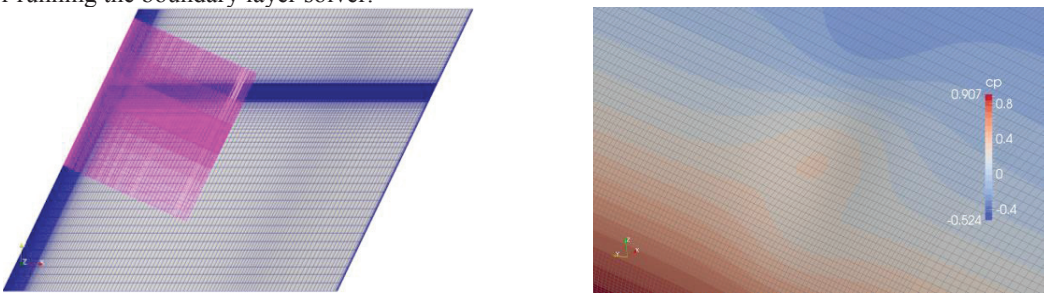

Fig. 3. Pressure cuts on RANS mesh (left) and interpolated pressure coefficient in dimple region (right).

3.3. Solutions to 3d boundary layer equations

An upper surface boundary layer solution marching from the attachment line was obtained on a uniform mesh spanning the region of extracted pressure data. This revealed streaks of enhanced/diminished displacement thickness components (δ_1 and δ_2) in the directions parallel and orthogonal to inviscid streamlines (Fig. 4) and contours of skin friction (Cf_1 and Cf_2) in the two directions (Fig. 5) indicating streaks of high and low speed flow near the wall and the collocated modulations in the cross flow component near the wall.

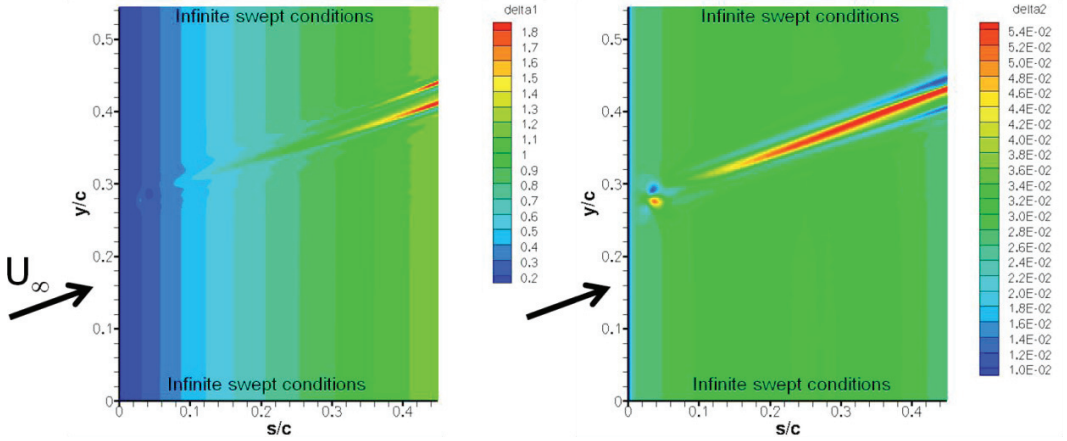

Fig. 4.Displacement thickness in (a) direction of inviscid streamlines; (b) orthogonal to inviscid streamline.

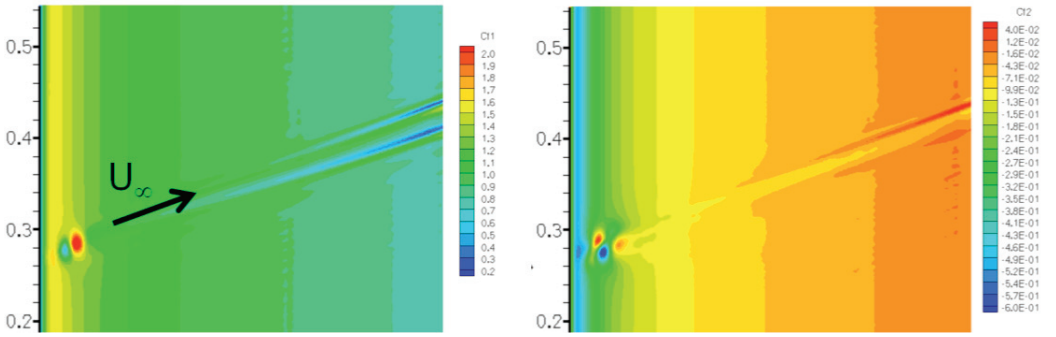

Fig. 5. Skin friction coefficient in (a) direction of inviscid streamlines; (b) orthogonal to inviscid streamline.

Filled velocity contours in a span-wise plane through the boundary layer at the most downstream region of the wake (Fig. 6) reveals regions of positive and negative wall normal vorticity indicating span-wise modulations in the wall tangential velocity. Line contours for wall normal velocity in the top right plot shows alternating regions of upwash and downwash flanking the wall normal vorticity which transfer high and low speed fluid across the boundary layer. This is seen in the line contours of the normal to leading edge component of wall tangential velocity (bottom right plot) where there are alternating regions of high and low speed flow near the wall. The bottom left plot shows the consequent variation in shear near the wall with region of high and low shear where there is flow towards and away from the wall. These features are consistent with counter-rotating longitudinal vortices through the wake region generating low and high speed streaks and modulations in the cross-flow.

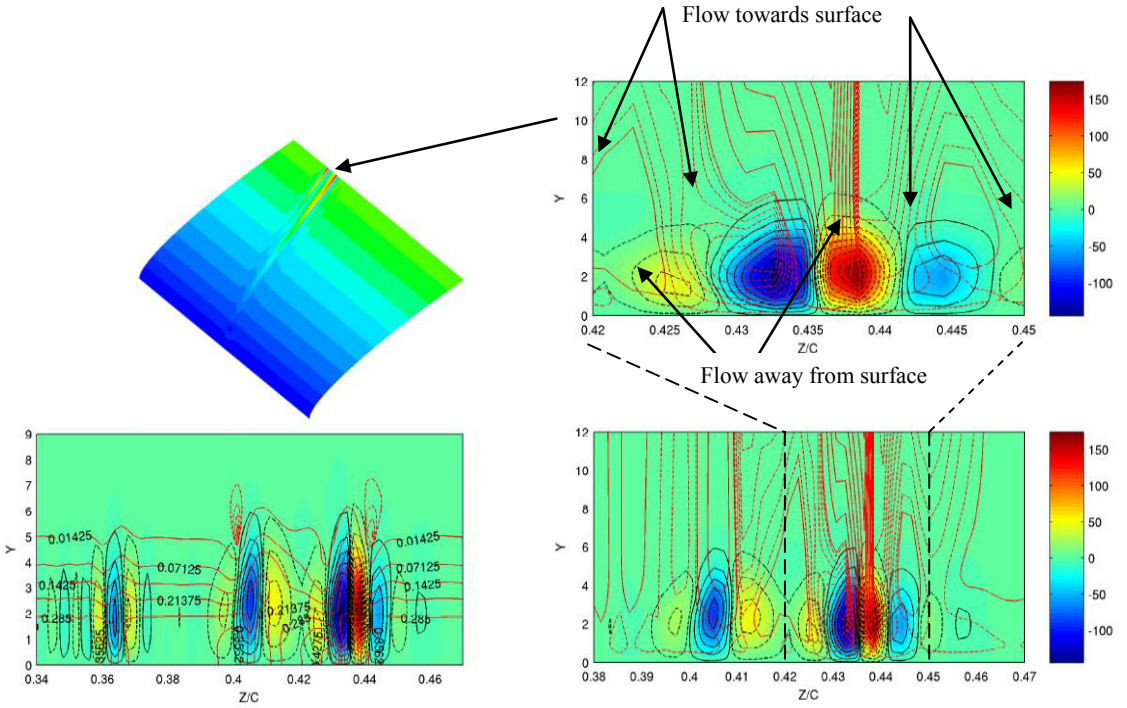

Fig. 6. Contours of wall normal vorticity with (top right) contour lines of wall normal velocity (bottom right) contours of wall tangential velocity (component normal to leading edge) and (bottom left) wall normal gradient of wall tangential velocity with broken lines for negative values.

3.4. Stability Analysis

The 3d parabolized stability equations were solved for span periodic unstable stationary cross-flow modes with wave-numbers in the range $1600 < \beta < 6000\text{m}^{-1}$ corresponding to span components of wavelength (in units of dimple diameter) in the range $1/8 < \lambda/d < 1/2$ i.e. the dimple was reasonable large compared to the wavelength of the unstable modes making a PSE based treatment valid.

An envelope analysis of maximum N factors and corresponding inflow span wave-number for both fully 3d and strip analysis is shown in Fig. 7. For the 3d analysis this reveals that in the infinite swept regions inboard and outboard of the dimple wake region there is a growth in maximum N factor up until about 20% chord after which all modes decay. Low wave-number modes with $\beta \cong 2000$ are the most amplified beyond this chord location. However in the wake region it is seen that high wave-number modes become unstable resulting in a rapid growth in maximum N factor. The corresponding inflow wave-number in this region is seen to diminishing as the span-wise extent of the region grows. A strip analysis is not able to capture the wake instability and instead produces a spurious horizontal region of high N factor behind the dimple.

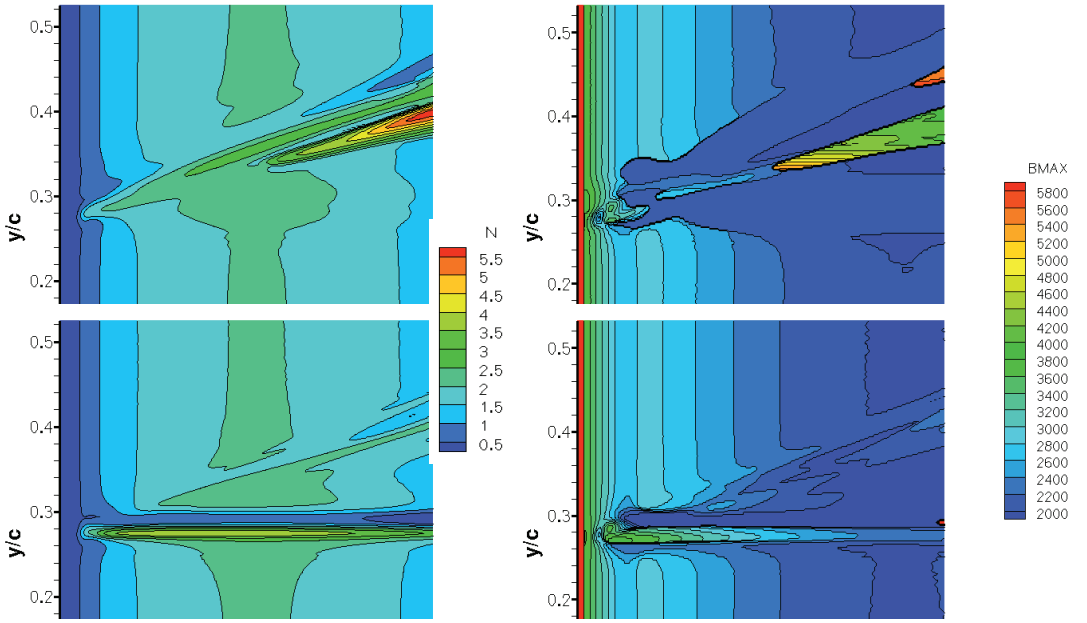

Fig. 7.PSE 3d analysis (top row) and PSE strip analysis (bottom row) with N factor envelope (left) and span-wise wave-number at inflow plane for mode with maximum N factor (right).

Growth rates for three span wave-numbers and both fully 3d analysis and strip analysis are shown in Fig. 8. For the 3d analysis there is almost no growth of the low wave-number mode β=2000 but there is a streak of strong growth of the higher wave-number modes β=4000 and β=6000 on the inboard side. Moving outboard a streak of high damping followed by another streak of a weaker growth streak accounts for the secondary peak in N factor seen in Fig. 7. For the strip analysis there is little growth in the wake. The line of perturbed N factor in Fig. 7 arises from the integration through the horizontally aligned peaks growth rates near the dimple.

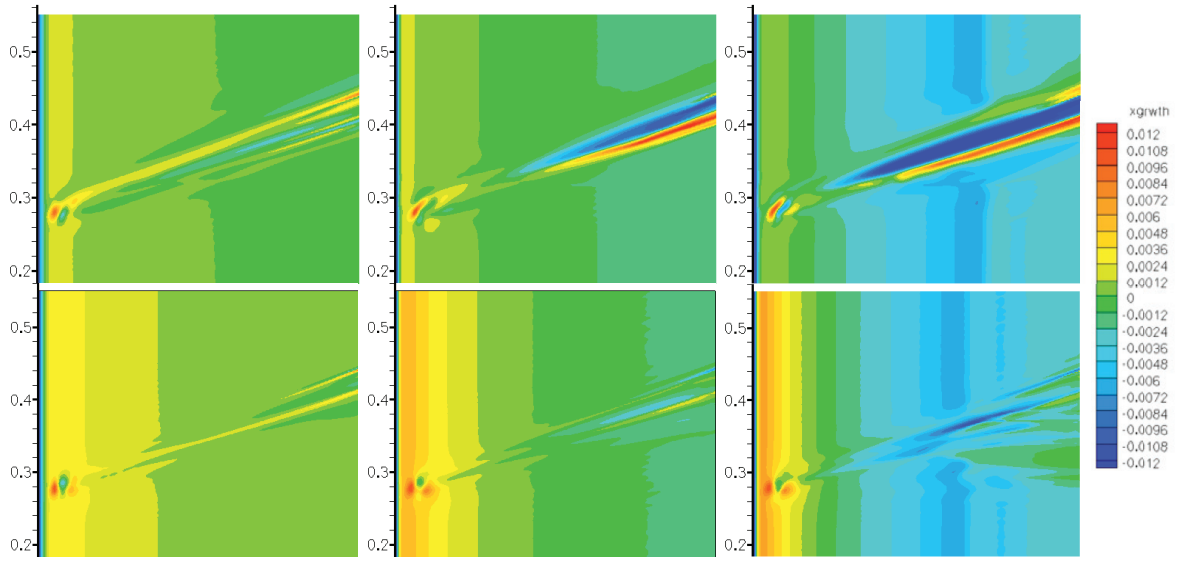

Fig. 8. PSE 3d analysis(top row) and PSE strip analysis (bottom row) with growth rate in direction normal to leading edge for span-wise wave-number β=2000 (left), β=4000 (middle) and β=6000 (right)

3.5. Marching in planes

For the periodic inflow states that have been considered the marching in planes method described in section 2.3 should produce identical results to the point to point marching scheme described in section 2.2 and used for the results above. Computations to confirm this is the case are in progress. One such computation is illustrated in Fig. 9 where it is seen that there is a good agreement in wave-number prediction for the case that has been examined (this is a non-stationary case with span wave-number β=2000 m^{-1} and frequency ω=2000Hz). Future work beyond comparing the methods periodic states will use the marching in planes method to look at bi-global localized instabilities arising in the dimple region.

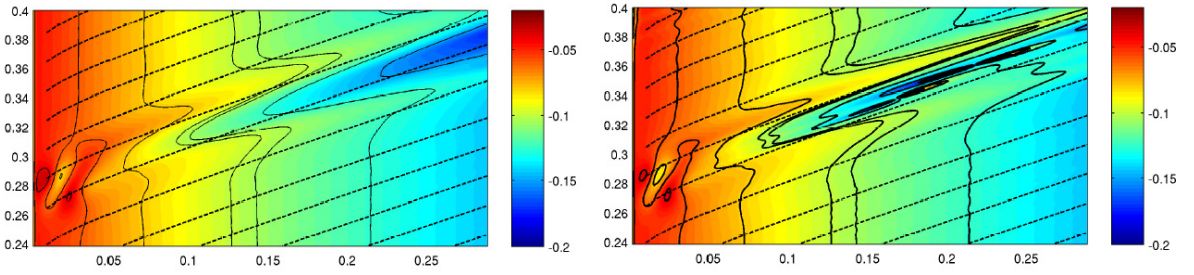

Fig. 9. Wavenumber α for β=2000m^{-1} and ω=2000Hz calculated with 3d point to point method (left) and marching in planes method (right). Broken lines indicate inviscid streamlines.

3.6. Conclusions

Fully three-dimensional methods for computing primary instabilities have been applied to a wing with flow conditions resembling those on a natural laminar flow wing with the addition of a leading edge dimple. It has been shown that a shallow dimple can be highly destabilizing to stationary cross-flow vortices potentially leading to early transition onset. The growth of instabilities occurs beyond about 20 per cent chord in longitudinal vortical structures within the boundary layer formed in the wake of the dimple Use of the standard strip approach based on a conical flow assumption and routinely used in the aerospace industry will give quite different results with no instability being seen in the wake. The point to point scheme used for the stability analysis is highly efficient and well suited for industrial use. First indications are that it agrees well with a more computationally intensive marching in planes approach

Acknowledgements

This work has been supported by the EPSRC funded LFC-UK project: Development of Underpinning Technology for Laminar Flow Control, grant EP/I037946/1 and by the TSB funded ALFET project.

References

1. Herbert T. On the stability of 3d boundary layers. AIAA Paper 1997-1961
2. Herbert T. Parabolized stability equations. Annu. Rev. Fluid Mech.-1997, Vol 29, pp245-283.
3. Mughal MS. Stability analysis of complex wing geometries: parabolised stability equations in generalised non-orthogonal coordinates. AIAA Paper 2006-3222.
4. Arthur M, Horton HP, Mughal MS. Modelling of natural transition in properly three-dimensional flows. AIAA Paper 2009-3556
5. Cebeci, T. and Cousteix, J. Modeling and Computation of Boundary-Layer Flows. ISBN-13: 978-3540244592. Springer, 2005.
6. Ashill PR, Betts CJ, Gaudet IM. A wind tunnel study of transonic flows on a swept panel wing at high subsonic speeds. CEAS 2nd European Forum on Laminar Flow Technology. 1996.
7. Leatham M, Stokes S, Shaw S, Cooper JA, Appa J, Blaylock T. Automatic mesh generation for rapid-response Navier-Stokes calculations. AIAA Paper 2000-2247